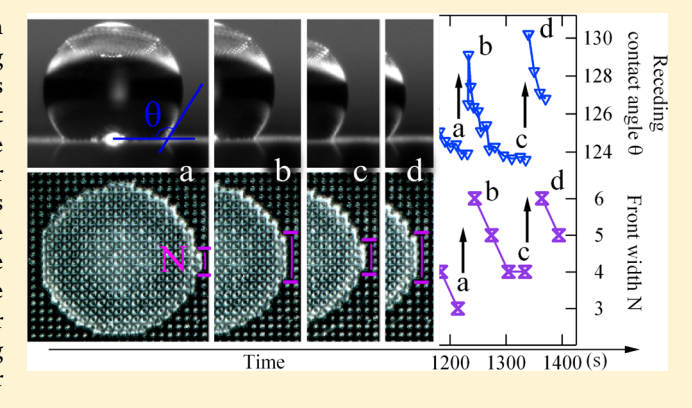


Finite Size Effects on Textured Surfaces: Recovering Contact Angles from Vagarious Drop Edges

Anaïs Gauthier, Marco Rivetti, Jérémie Teisseire,* and Etienne Barthel*

Surface du Verre et Interfaces, UMR 125 CNRS/Saint-Gobain, Aubervilliers, France

ABSTRACT: A clue to understand wetting hysteresis on superhydrophobic surfaces is the relation between receding contact angle and surface textures. When the surface textures are large, there is a significant distribution of local contact angles around the drop. As seen from the cross section, the apparent contact angle oscillates as the triple line recedes. Our experiments demonstrate that the origin of these oscillations is a finite size effect. Combining side and bottom views of the drop, we take into account the 3D conformation of the surface near the edge to evaluate an intrinsic contact angle from the oscillations of the apparent contact angle. We find that for drops receding on axisymmetric textures the intrinsic receding contact angle is the minimum value of the oscillation while for a square lattice it is the maximum.



■ INTRODUCTION

Surface roughness and textures are known to dramatically modify the wetting properties of a solid, especially enhancing superhydrophobicity. For a small liquid droplet lying on a textured surface, the Cassie¹ and Wenzel² models generalize the classical Young theory based on the global equilibrium of the triple line.³ However, the limits of equilibrium models have been pointed out repeatedly. Beyond thermodynamic equilibrium, a key point has emerged in the past 10 years: the presence of metastable states and pinning, which has put emphasis on the role of the local conformation of the triple line.⁵ Some recent developments have tried to take into account this local conformation to improve the classical thermodynamic theories⁶⁻⁸ while others have proposed pinning theories where the interplay between surface heterogeneities and the deformability of the triple line is considered explicitly. 9-12

In parallel to this controversy, the presence of heterogeneities all along the triple line has significant experimental consequences. Indeed, it is well-known that surface textures induce a distribution of local contact angles along the perimeter of the drop. On many superhydrophobic surfaces, the texture size is in the 10 μ m range: with such large textures the distribution of local angles spreads over several degrees. During a contact angle measurement the measured contact angle is found to vary somewhat jerkily as the triple line recedes because of the local contact angle distribution around the drop. In fact, what is reported is an oscillatory evolution of the contact angle with time. 13-15 The question that arises is, which one is the physically meaningful receding contact angle: the minimum value, the maximum, or the average?

In a detailed investigation of receding triple lines on textured surfaces, McHale et al. 3 measured the contact angle oscillations

quantitatively. They ascribed the oscillations to a "step-like retreat" induced by the finite size of the texture. They analyzed the oscillations with an axisymmetric pinning model¹⁶ and were able to reasonably account for the amplitude of the oscillations. However, they did not provide insight into which value of the measured contact angle is physically meaningful.

In this paper we report on an in-depth investigation of these oscillations of the contact angle. We have studied the time evolution of the receding contact angle on superhydrophobic surfaces textured with distributions of posts. Two types of surfaces were compared: a regular surface with periodic texture and a more unusual surface with axisymmetric features. Also, for a better understanding of the relation between triple line morphology and receding contact angle, we have introduced a primitive 3D visualization of the drop shape. With this additional input on the local conformation of the triple line, we can compare the origins of the oscillations on the axisymmetric and periodic surfaces, which are quite different. We show that in each case a meaningful value of the macroscopic contact angle can be recovered from the seemingly erratic evolution of the measured contact angle.

MATERIALS AND METHODS

Following the method previously described in refs 11 and 12, hydrophobic surfaces are obtained by spin-coating a hybrid silica layer on a glass surface with a sol-gel process. The texture is imprinted using an elastomeric mold, and hydrophobicity is enhanced by silanization.

September 27, 2013 Received: Revised: December 17, 2013



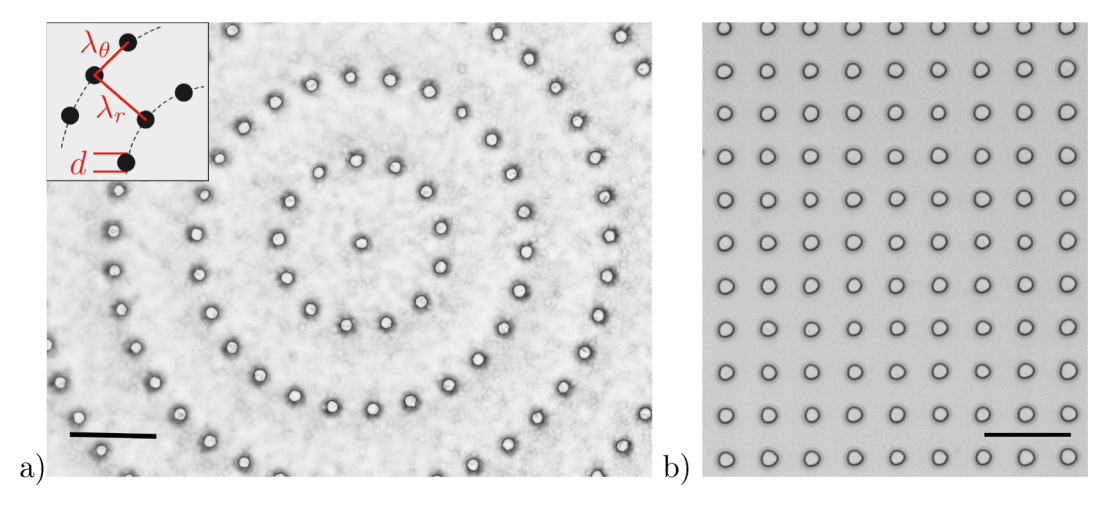


Figure 1. Textures and geometrical parameters for: (a) an axisymmetric surface (dartboard) with radial period $\lambda_r = 60 \ \mu m$ and tangential period $\lambda_{\theta} = 30 \ \mu m$; (b) a periodic surface (checkerboard) with period $\lambda = 30 \ \mu m$. For both surfaces the pillar diameter is $d = 10 \ \mu m$, and the scale bar is $60 \ \mu m$.

The textures are obtained with cylindrical 10 μ m diameter posts arranged in two different patterns. The first pattern (Figure 1a) consists of concentric circles, in the manner of a dartboard. It is axisymmetric, and the distance between two circles (radial period) is $\lambda_{\rm r}=60~\mu{\rm m}$. The distance between two adjacent posts (tangential period) is $\lambda_{\theta}=30~\mu{\rm m}$. The second pattern consists of a square lattice (Figure 1b), in the manner of a checkerboard. It is translationally invariant, with a period $\lambda=30~\mu{\rm m}$.

The liquid used in all the experiments is water. The typical initial drop volume is about 5 μ L, and evaporation takes place at normal conditions (atmospheric pressure and room temperature). We do not control the temperature or humidity, as we focus our attention on the kinematics of the triple line and not on the evaporation kinetics.

We monitor the evaporation of the droplet from two different directions simultaneously. From the side view (Figure 2, top) the contact angle θ , contact radius r, and drop height h are measured. For periodic surfaces, the side views are taken along the row directions. Thanks to the transparency of the substrate, we can also monitor the

contact area: from the bottom view (Figure 2 bottom) the conformation of the triple line is assessed. In practice, the droplet actually sits upside down for easy observation of the bottom view with an ordinary microscope. The droplet is first deposited on an ultralow adhesion surface and then transferred to the surface of interest where it remains suspended during evaporation.

RESULTS

Our observations of drop shapes during evaporation are summarized in spatiotemporal plots (Figures 3 and 6) displaying the evolution of the drop base (horizontal cross section, top plot) and drop height (vertical cross section, bottom plot). These plots are obtained using the "orthogonal views" command in the ImageJ software. The spatiotemporal plots reveal the overall shrinkage of the drop before the drop transits to fully wetting in the Wenzel state.

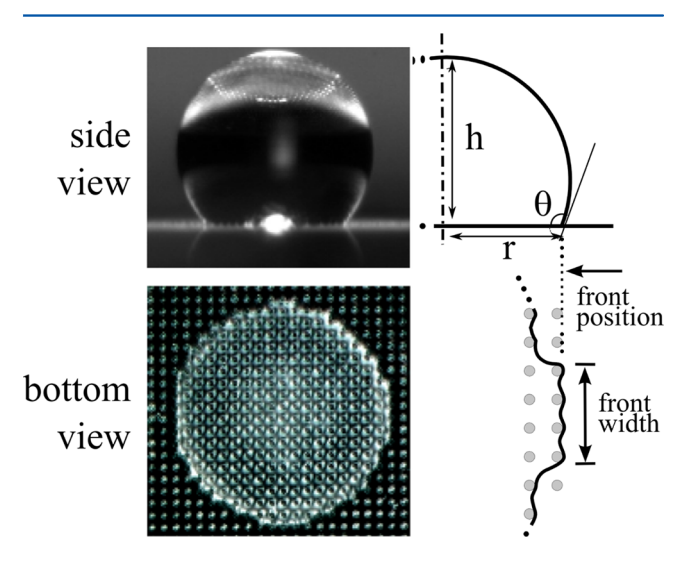


Figure 2. Experimental arrangement: the side view and the bottom view are recorded simultaneously. From the side view, contact angle, drop radius and height can be measured. From the bottom view, the conformation of the triple line on the surface textures is evaluated. In the present instance, the surface texture is a square array. At the edge of the drop, the triple line is seen to sit on the outermost row, which defines the front position. The front width is defined by the number of posts wetted by the triple line on this row.

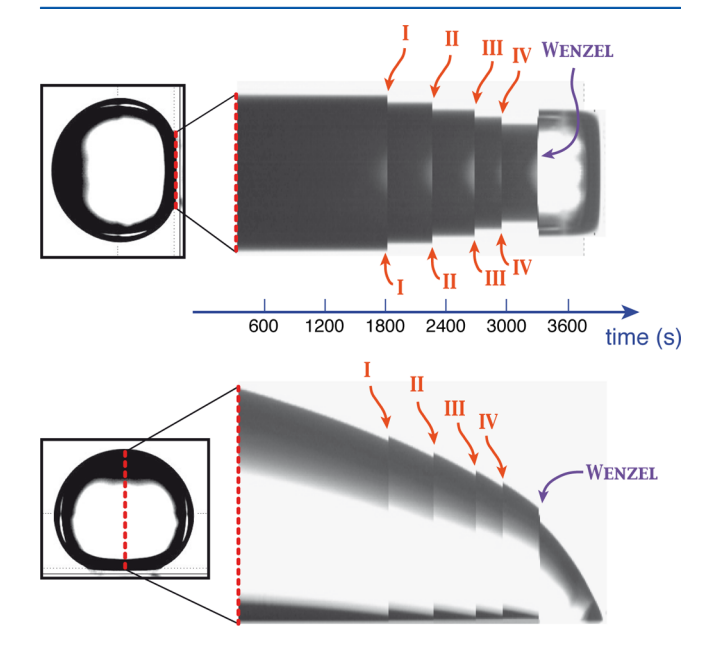


Figure 3. Spatiotemporal plot of drop morphology as a function of time: (top) horizontal cross section through the base of the drop and (bottom) vertical cross sections on a dartboard surface. Contact radius jumps on both sides of the cross section and height jumps (denoted I-IV) all occur simultaneously.

On the axisymmetric surface the drop first self-centers (not shown) until the edge sits exactly on a circle of pillars. This transient phase lasts for a variable amount of time, depending on the marksmanship of the operator. Once the drop has centered, we observe a series of jumps affecting the drop rim (labeled I to IV in Figure 3, top), separated by phases where the base radius stays constant. Quite surprisingly, observation of the drop profile shows that the jump of the rim leads to a concomitant jump of the drop height (Figure 3, bottom).

We also plot the time evolution of the contact angle and the position of the edge of the drop in Figure 4. The receding

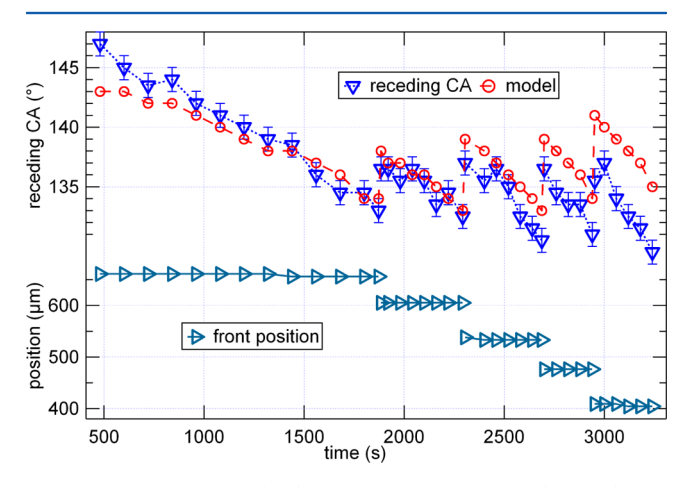


Figure 4. Contact angle (top) and drop edge position (bottom) as a function of time for an axisymmetric (dartboard) surface. Also shown in the top panel is the prediction for the contact angle based on measured contact radius and drop height (eq 4).

contact angle increases suddenly with each contact radius jump. Between jumps the contact angle and drop height both decrease gently. The overall picture, confirmed by the bottom views (not shown), is that of a series of jumps affecting the whole drop edge simultaneously (Figure 5a). Since this sudden retraction of the triple line by a distance equal to the radial period of the texture (Figure 4, bottom) occurs at constant volume, it is accommodated by a sudden increase of both

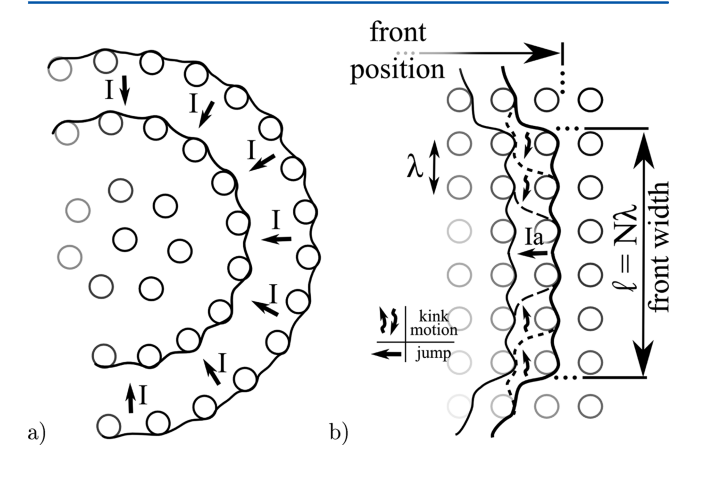


Figure 5. (a) Drop edge kinematics for axisymmetric surfaces. When the drop recedes, the triple line stays pinned on a circle of pillars. When the jump occurs, it involves the triple line as a whole. (b) Drop edge kinematics for periodic surfaces. When the drop recedes, the protrusion shrinks through the motion of two opposite kinks. When the protrusion is too narrow, it jumps on the inner row of pillars.

height (Figure 3, bottom) and contact angle (Figure 4, top). Between jumps, a smooth decrease is observed as the drop shrinks gradually at constant contact radius.

For the periodic surface, we also find a stepwise evolution of the contact radius (Figure 6). However, we find that the jumps on opposite sides of the rim (labeled Ia–IVa on one side and Ib–Vb on the other side) are clearly not synchronized. Our data also evidence the usual continuous decrease of the drop height (Figure 6, bottom), without any sign of height jump.

These results point to quite a different mechanism. For the axisymmetric texture, the drop can naturally sit on a circle of pillars. For the periodic texture, the triple line conformation is more elaborate: because of geometrical incompatibility between the axisymmetric drop and the periodic texture, the triple line must deform in locations where it bends out of a given row of pillars into the next (Figure 2, bottom). This deformation is a defect which we have previously called a kink. The edge of the drop can then be seen as a protrusion delimited by two opposite kinks. The local geometry (Figure 5b) can be defined by the position of the protrusion (the row on which the protrusion sits) and the width of the protrusion (the distance between the two opposite kinks). This distance is best measured as a number of pillars N, equivalent to a length $l = N\lambda$.

Plotting the time evolution of the contact angle and the front position (Figure 7, top and middle), we find that they are quite

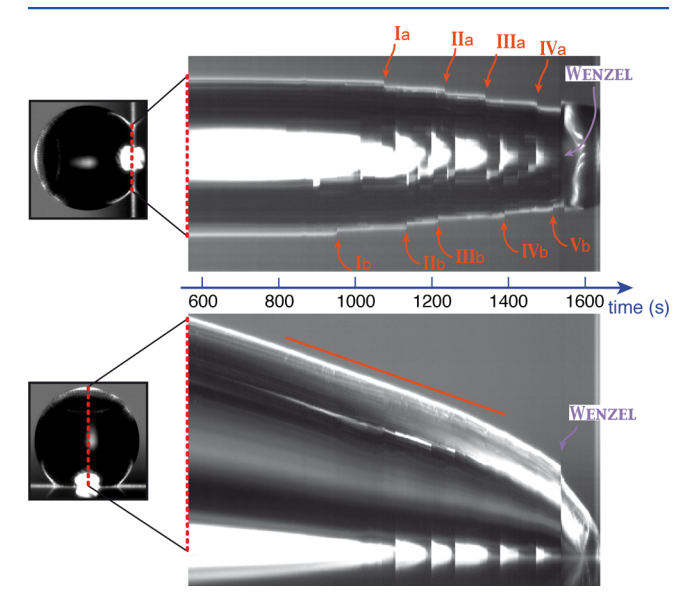


Figure 6. Same spatiotemporal plot of drop morphology as a function of time for a checkerboard surface. As in the previous case, position jumps also affect the edge. They are denoted I—IVa on one side of the cross section and I—Vb on the other side. There is no time correlation between jumps across the drop. The drop height decreases smoothly, without any measurable jump.

similar to the evolution observed in the axisymmetric case. However, when we plot the front width (Figure 7, bottom) as recorded from the bottom view, we find that the decrease of the contact angle is related to the decrease of the front width. More precisely, as the protrusion becomes narrower the contact angle decreases. This evolution takes place until the narrow protrusion suddenly jumps and settles as a significantly wider protrusion on the next row, thus changing position by one row inward (Figure 5b).

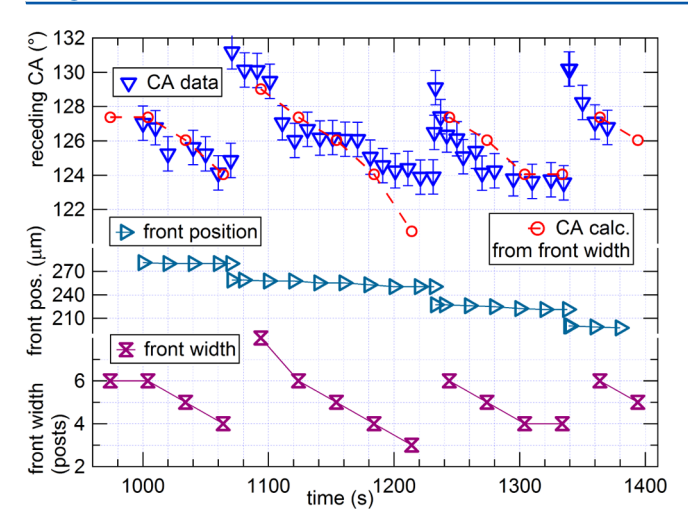


Figure 7. Contact angle (top), drop edge position (middle), and front width (bottom) as a function of time for a periodic (checkerboard) surface. Also shown in the top panel is the prediction for the contact angle based on measured front width (eq 5).

Despite clear similarities in the time evolution of contact angle and jumps, it appears that the axisymmetric and the periodic surfaces differ significantly. For an axisymmetric surface liquid redistribution during the jump involves the full drop, as evidenced by correlation across the drop and height jump. For a periodic surface, this is a much more local affair which involves a protrusion which typically extends over a few pillars.

DISCUSSION

We now develop a quantitative analysis of the data.

Consider first the axisymmetric case. In the spherical cap model, the drop volume as a function of contact radius r and contact angle θ is

$$V = \frac{\pi r^3}{3} \frac{(1 - \cos \theta)^2 (2 + \cos \theta)}{\sin^3 \theta} \tag{1}$$

When the triple line is pinned (constant r), a progressive reduction of drop volume through evaporation leads to a decrease of the contact angle. Following McHale et al., ¹³ we consider a sudden (small) jump of the radius from $r \rightarrow r - \delta r$. Since this change is rapid, it occurs at constant volume. From eq 1 the contact angle variation is

$$\delta\theta = \sin\theta(2 + \cos\theta) \frac{\delta r}{r} \tag{2}$$

which was found to provide a reasonable evaluation of the contact angle jumps. 13

To analyze the height jumps, we carry out identical calculations substituting the drop height h for the contact angle θ . A (small) change in the radius $r \to r - \delta r$ leads to a (small) change in the height $h \to h + \delta h$ with

$$\delta h = \frac{2rh}{r^2 + h^2} \delta r \tag{3}$$

For an axisymmetric drop, δh is expected to be of the same order of magnitude as δr . Predictions given by eqs 2 and 3 are in good agreement with the experimental observations, with predicted values $\delta\theta=6.7^{\circ}$ and $\delta h=40~\mu m$. We can also test the

validity of the axisymmetric model in another way. The circular arc relation for the cross section of the drop is

$$\tan\frac{\theta}{2} = \frac{h}{r} \tag{4}$$

and this relation between contact angle, contact radius, and drop height is consistent with the experimental results (Figure 4, top curve). Nevertheless, while the oscillations are indeed correctly reproduced by eq 4, we also observe an overall drift which is not predicted by the model. Indeed, it becomes less and less accurate to assume that the geometry is axisymmetric as the triple line moves inward, due to the finite diameter of the posts.

However, for periodic surfaces, the axisymmetric model is clearly inadequate. In this case, the jumps of the contact radius are not correlated across the drop, and there is no height jump. These observations make sense since the jumps are local and do not involve liquid redistribution at the drop scale as for axisymmetric surfaces. We therefore propose a different model for contact angle jumps.

Focusing on the local conformation of the triple line, we follow Joanny and de Gennes: ¹⁷ for an in-plane perturbation of the triple line of width l, the perturbation of the liquid surface decreases exponentially with a decay length of the order of l along the out-of-plane direction (Figure 8). In our problem, the

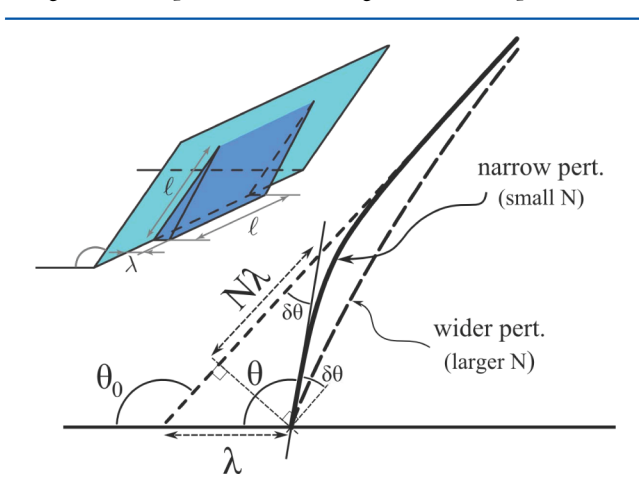


Figure 8. Schematic of the drop edge deformation: local contact angle resulting from an in-plane perturbation of the triple line (width $l = N\lambda$) approximated from a simple geometrical construction. Inset: as a result of equilibrium of the drop surface, an in-plane perturbation of the triple line (width l) decays in the perpendicular direction (i.e., along the surface of the drop) over a characteristic distance equal to l.

protrusions of the front are observed in the bottom view (Figures 2 and 5b). The width of the protrusion is $l=N\lambda$, and this distance sets the out-of-plane extent of the perturbation (Figure 8), according to the Joanny and de Gennes theory. Owing to this protrusion of finite size, the contact angle θ measured near the surface differs from the contact angle θ_0 measured away from the surface. The difference $\delta\theta$ can be easily calculated by projection (Figure 8). We find that $\delta\theta=\theta_0-\theta\simeq\lambda\sin\theta_0/(N\lambda)$, so that the relation between θ , θ_0 , and N is

$$\theta = \theta_0 - \frac{\sin \theta_0}{N} \tag{5}$$

We have observed that the contact angle θ decreases when the width of the perturbation decreases. This trend is fully consistent with the geometrical argument we propose, as shown in Figure 8 and evidenced by eq 5. With this equation, we can use the measured values of N to calculate the contact angle oscillations with only one free parameter θ_0 . Results for θ_0 = 134° are displayed in Figure 7 and show good agreement with the measured contact angle values. We conclude that this simple approach adequately reproduces the oscillations of the contact angle, even if it does not take into account the finer details of the conformation of the pinned triple line, such as the exact position of the line on the pillars or the shape of the pillar. When $N \to \infty$, the spatial extent of the protrusion diverges and the correction to the contact angle drops to zero. In this case the measured receding contact angle converges to θ_0 , which stands out as an intrinsic contact angle, unaffected by finite size effects. This angle θ_0 determines the threshold tension which has to be applied to the triple line in order to just obtain depinning, for an infinitely large drop. In principle, θ_0 could be measured far away from the surface, where all the finite size perturbations due to surface textures have decayed to zero. However, we have to keep the drop size smaller than the capillary length, that is to say, in the ~1 mm range or smaller, while the typical triple line perturbations extend over a few lattice parameters, in the $\sim 100 \ \mu m$ range. As a result, the natural curvature of the drop makes it nearly impossible to measure the intrinsic contact angle θ_0 far enough from the surface. In short, it is to be expected that the contact angle measurement is quite generally affected by finite size effects for textures in the range of 10 μ m or more, and it turns out difficult to evaluate the intrinsic contact angle θ_0 : extrapolating as a function of perturbation size as we have done here is a viable way to reach that goal. In contrast, for an axisymmetric surface the size of the perturbation is actually the drop size. Once the depinning threshold is reached, the contact radius, the contact angle and the drop height all jump simultaneously, as accurately rendered by the axisymmetric model.

Once the oscillations have been measured, how do we determine the receding contact angle? Let us first consider the axisymmetric texture. The measured contact angle is at a minimum just before the jump. At this point the tension on the triple line is maximum, and the triple line depins as a whole. This depinning threshold depends upon pillar geometry and tangential period λ_{θ} in a manner discussed before.^{7,12} Since the triple line sits perfectly on the circle of pillars, without any kink, the radial period λ_r does not affect the depinning threshold: how much the line will have to jump after it has depinned is of course irrelevant to the threshold itself! Just after the jump, however, there is a sudden excess volume, and the contact angle is now at a maximum. It has increased by a value given by eq 2. Since $\delta r = \lambda_r$, the contact angle just after the jump primarily depends upon the radial period. Clearly in this case the intrinsic contact angle is the depinning contact angle, i.e., the minimum value, while the maximum contact angle, which depends upon parameters to which pinning is indifferent, has no intrinsic character. The general picture which emerges is that the jump leaves the system with some surplus volume: subsequent evaporation will gradually bring the contact angle down to the intrinsic depinning threshold whereupon the next jump occurs. Let us now turn to the periodic surface; it would be tempting to assume that the same occurs in this case. However, the present results suggest that when a drop sits on a periodic texture, the resulting protrusion on the edge interferes with contact angle in

the opposite manner. The effect of the protrusion is to reduce the contact angle by an amount which is inversely proportional to the protrusion width, so that for a periodic surface we expect that it is the maximum contact angle which is closest to the intrinsic contact angle.

CONCLUSIONS

In this paper we have considered the evaporation of liquid droplets on textured surfaces. In particular, we have monitored the evolution of the contact radius, drop height, and contact angle on both an axisymmetric surface and a periodic surface.

For the axisymmetric surface, the triple line is pinned on a row of posts and the contact angle decreases as the drop evaporates. At the threshold angle, depinning occurs, affecting the full contact line simultaneously. We have shown that the axisymmetric model accurately captures this kinematics with simultaneous jumps of the contact radius, drop height, and contact angle upon depinning. In this case the intrinsic receding contact angle is the *minimum* contact angle, for which the tension applied to the triple line is maximum.

For a periodic texture, local distortions of the triple line form protrusions which extend in the out-of-plane direction up to a distance of the order of the in-plane width. When the receding contact angle is measured during evaporation, the recorded oscillations are due to the periodic evolution of these protrusions as they adjust while the triple line recedes.

Here we have shown that by taking into account the full 3D shape of the drop, even in a rather coarse way, the spatial extent of the perturbation can be assessed and the contact angle value can be corrected for finite size effects to evaluate the intrinsic contact angle. Our results demonstrate that in this case it is the *maximum* value which lies closest to the intrinsic receding contact angle.

This contrasted behavior provides another demonstration of the central role played by the local configurations of the triple line and associated metastable states in wetting problems. It also highlights the necessity to think in three dimensions, since it is from the conformation of the liquid surface around the drop edge that we can make sense of the in-plane configuration of the triple line itself.

AUTHOR INFORMATION

Corresponding Authors

*E-mail jeremie.teisseire@saint-gobain.com (J.T.).

*E-mail etienne.barthel@saint-gobain.com (E.B.).

Present Address

A.G.: LadHyX, UMR 7646 Ecole Polytechnique & CNRS, Palaiseau, France.

Notes

The authors declare no competing financial interest.

REFERENCES

- (1) Cassie, A.; Baxter, S. Wettability of porous surfaces. *Trans. Faraday Soc.* **1944**, 40, 546–551.
- (2) Wenzel, R. N. Resistance of solid surfaces to wetting by water. Ind. Eng. Chem. 1936, 28, 988-994.
- (3) De Gennes, P.-G.; Brochard-Wyart, F.; Quéré, D. Capillarity and Wetting Phenomena: Drops, Bubbles, Pearls, Waves; Springer: Berlin, 2004
- (4) Gao, L.; McCarthy, T. J. How Wenzel and Cassie were wrong. Langmuir 2007, 23, 3762–3765.
- (5) Quéré, D. Rough ideas on wetting. Physica A 2002, 313, 32-46.

(6) Extrand, C. Model for contact angles and hysteresis on rough and ultraphobic surfaces. *Langmuir* **2002**, *18*, 7991–7999.

- (7) Choi, W.; Tuteja, A.; Mabry, J. M.; Cohen, R. E.; McKinley, G. H. A modified Cassie—Baxter relationship to explain contact angle hysteresis and anisotropy on non-wetting textured surfaces. *J. Colloid Interface Sci.* **2009**, 339, 208–216.
- (8) Raj, R.; Enright, R.; Zhu, Y.; Adera, S.; Wang, E. N. Unified model for contact angle hysteresis on heterogeneous and superhydrophobic surfaces. *Langmuir* **2012**, *28*, 15777–15788.
- (9) De Gennes, P.-G. Wetting: statics and dynamics. Rev. Mod. Phys. 1985, 57, 827.
- (10) Reyssat, M.; Quere, D. Contact angle hysteresis generated by strong dilute defects. *J. Phys. Chem. B* **2009**, *113*, 3906–3909.
- (11) Dubov, A.; Teisseire, J.; Barthel, E. Elastic instability and contact angles on hydrophobic surfaces with periodic textures. *Eur. Phys. Lett.* **2012**, *97*, 26003.
- (12) Gauthier, A.; Rivetti, M.; Teisseire, J.; Barthel, E. Role of kinks in the dynamics of contact lines receding on superhydrophobic surfaces. *Phys. Rev. Lett.* **2013**, *110*, 046101.
- (13) McHale, G.; Aqil, S.; Shirtcliffe, N.; Newton, M.; Erbil, H. Analysis of droplet evaporation on a superhydrophobic surface. *Langmuir* **2005**, *21*, 11053–11060.
- (14) Anantharaju, N.; Panchagnula, M.; Neti, S. Evaporating drops on patterned surfaces: Transition from pinned to moving triple line. *J. Colloid Interface Sci.* **2009**, 337, 176–182.
- (15) Orejon, D.; Sefiane, K.; Shanahan, M. E. Stick—slip of evaporating droplets: Substrate hydrophobicity and nanoparticle concentration. *Langmuir* **2011**, *27*, 12834–12843.
- (16) Shanahan, M. E. Simple theory of "stick-slip" wetting hysteresis. *Langmuir* **1995**, *11*, 1041–1043.
- (17) Joanny, J.; de Gennes, P. A model for contact angle hysteresis. *J. Chem. Phys.* **1984**, *81*, 552.